Journal of Sol-Gel Science and Technology (2025) 114:386–398
https://doi.org/10.1007/s10971-025-06678-9

ORIGINAL PAPER

Structural and gas sensing properties of NiO thin films deposited by a novel spin coating technique

Enes Nayman[1] · Mehmet Fatih Gozukizil[1] · Bayram Armutci[1] · Sinan Temel[2] · Fatma Ozge Gokmen[3]

Received: 10 October 2024 / Accepted: 18 January 2025 / Published online: 11 February 2025

Abstract

This study presents the development and application of a novel sol-gel spin coating technique for the deposition of nickel oxide (NiO) thin films on glass substrates. The newly designed spin coating device operates without the need for a vacuum, providing a cost-effective alternative to traditional methods. NiO thin films were prepared using a sol-gel process, with various thicknesses and rotation speeds tested to idealize film quality. Structural and morphological analyses were conducted using X-Ray Diffraction (XRD) and Field Emission Scanning Electron Microscopy (FESEM), revealing that the 6-layer sample coated at 3000 rpm exhibited the best crystallization and surface homogeneity. Gas sensor tests were performed to evaluate the sensitivity of the NiO thin films to ethanol, NO_2, and H_2 gases. The results showed that the sensor responded stably and reproducibly over multiple gas exposure cycles. It also demonstrated the potential for reliable gas detection applications.

Graphical Abstract

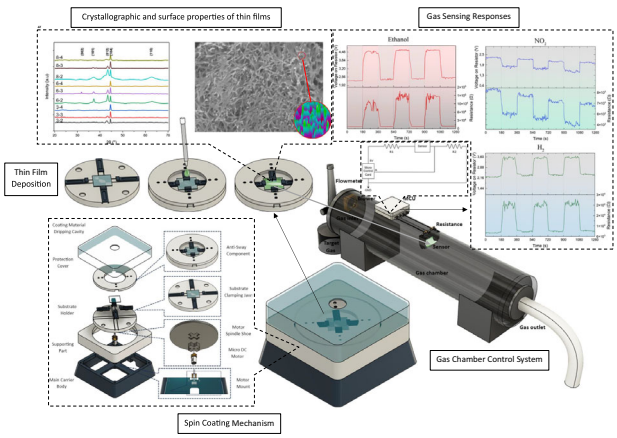

Keywords NiO thin films · Spin coating · Sol-gel · Gas sensors · Nanomaterials

Highlights

- A novel cost-effective and vacuum-free sol-gel spin coating device was developed for NiO thin film deposition.
- NiO thin films produced at 3000 rpm with 6 layers showed the best crystallization and surface homogeneity based on XRD and FESEM analyses.
- The films demonstrated sensitive, stable, and repeatable performance in detecting ethanol, NO_2, and H_2 gases.
- The structural and surface properties of NiO thin films significantly influenced gas sensing performance, with the 6-layer series yielding the best results.

✉ Enes Nayman
enes.nayman@bilecik.edu.tr

[1] Sogut Vocational School, Bilecik Seyh Edebali University, Sogut, Bilecik 11600, Turkey

[2] Physics Department, Bilecik Seyh Edebali University, Street, Bilecik 11000, Turkey

[3] Vocational School, Bilecik Seyh Edebali University, Street, Bilecik 11000, Turkey

1 Introduction

Today, environmental pollution has become a source of concern as it not only has negative effects on human health but also prevents the consumption of natural resources [1–3]. One of the environmental pollutants is air pollution. Harmful gas emissions are one of the leading factors that cause air pollution [4]. Sensors with sensing and warning features are used to detect all these harmful gases [5–9]. One of the most widely used sensors is semiconductor sensors [10–13]. Semiconductor materials coated as thin films are obtained with the help of different deposition processes [14–19]. Different methods such as dip coating [20, 21] spin coating [22–25] spray pyrolysis [26], chemical bath deposition [27–29], physical [30, 31] and chemical vapor deposition [32] are applied both singly and in hybrid form [33, 34]. The wide variety of these methods allows coating the surfaces of materials with different structural and surface properties [35–37]. It is of great importance to choose the most ideal method according to the function of the material to be coated as a thin film and to ensure that the parameters of this method provide optimum conditions for deposition [38, 39]. Apart from the methods, the substrates and deposition materials to be used in thin film deposition applications are also of great importance for the course of the study [40–42]. In the production of semiconductor sensors, oxide films are frequently used as semiconductor materials [43, 44]. In particular, metal oxide semiconductors are preferred for their fast production processes, easy integration on different surfaces, economical and portable [45]. Nickel oxide (NiO) is widely used in photovoltaic [46–48] and sensor studies in the field of electronics [49–51]. In this study, an innovative approach to the spin coating method widely used in the literature has been introduced. The new low-cost and vacuum-free spin coating device developed offers results that are compatible with the speed, performance and sensitivity values of existing methods. Thin films deposited with the new spin coating mechanism developed as an alternative to conventional methods can be used in different applications such as sensors, optoelectronic materials, photovoltaics. In this study, NiO thin films were originally deposited with different parameters with the new method developed for both device design and different thin film applications. The structural and morphological properties of NiO thin films deposited on glass substrates were analysed by X-Ray Diffraction (XRD) and Field Emission Scanning Electron Microscopy (FESEM). The thin films were also tested as gas sensors against ethanol, NO_2, and H_2 gases. Therefore, the study is considered to be an innovative and important contribution to the fields of both materials science and sensor technology.

2 Material and method

NiO metal oxide semiconductor solutions were prepared and thin film deposition was carried out on the surfaces of glass samples. NiO thin films were coated on glass samples with the new alternative spin coating method we developed. The chemical synthesis recipe used in the study was created by examining reference studies in the literature on metal oxides (NiO etc.) thin film production and passing through certain optimization processes [52–57]. Nickel(II) Nitrate Hexahydrate [$Ni(NO_3)_2 \cdot 6H_2O$] was selected as the starting material for the production of NiO thin films. This material was preferred due to its high purity and ease of solubility and processing. While preparing the solution, nickel nitrate was dissolved in 2-Methoxyethanol and some Monoethanolamine was added to the solution to provide stabilization. Monoethanolamine both increases the homogeneity of the solution with its ability to chelate metal ions and has an improving effect on the crystallization of the films. Chemical calculations were carried out to produce 0.5 M NiO thin film as a product of the reaction. 7.27 g of Nickel(II) Nitrate was added to 50 ml of 2-Methoxyethanol in a beaker to form 0.5M NiO solution. The mixture was stirred together at 60 ℃ for 30 min. Then, 4 drops of monoethanolamine were added to the mixture. Stirring continued at 60 ℃ for 2 h. The prepared solution was kept at room temperature for 1 day and was ready for deposition. NiO thin films were prepared by spin coating on glass substrates by sol-gel technique. Samples of various thicknesses (3, 6 and 8 layers) were prepared at different rotation speeds (2000, 3000 and 4000 rpm). As a result of the experiments, 9 different samples were obtained. Each repetition was performed by spinning for 30 s, with a 2-min intermediate annealing process after coating. The samples were finally annealed in air at 400 ℃ for 2 h for calcination. The serial names of these samples and the applied processes are shown in Table 1.

There are different studies on the decomposition of nickel nitrate hexahydrate to nickel oxide. The common view of these studies is the simultaneous loss of water and nitrogen oxides (N_2O_5,NO_2) during decomposition. Firstly, dehydrated nickelnitrate products are obtained by heat treatment. On the other hand, if some water remains in the ambient, the products gradually form basic nickel nitrate complexes such as $Ni(NO_3)_2$:$Ni(OH)_2$ during the heat treatment. When the ambient pH is measured, it is reported that NiO is formed as a result of hydropyrolytic reactions gradually throughout the heat treatment. In the magnetic spin coating process, the process that takes place between the solution and the substrate is physisorption. The fact that this physisorption is strong before annealing is due to the gradual decomposition products affecting the ambient pH in the first step reaction. As a result of hydropyrolytic

Table 1 Layers and RPM for different serial samples

Serial	Number of layers	Rotation speed (Rpm)
3-2	3	2000
3-3	3	3000
3-4	3	4000
6-2	6	2000
6-3	6	3000
6-4	6	4000
8-2	8	2000
8-3	8	3000
8-4	8	4000

reactions, basic nickel nitrate species are formed [58]. Nickel(II) Nitrate Hexahydrate is often used as a precursor in the formation and preparation of NiO thin film. The decomposition reactions for NiO film formation are given in the following equations. In these equations, the mechanism of NiO production on glass substrate by a two-step reaction approach is proposed. The first reaction is the hydro-pyrolytic decomposition reaction in sol-gel solution and the second reaction is the calcination process decomposition reaction. The second reaction is complementary to the first reaction and is the calcination step necessary for the formation of the NiO crystalline phase [59].

1st step: hydropyrolitic reaxions.

$$2Ni(NO_3)_2 \cdot 6H_2O + CH_3OCH_2CH_2OH \xrightarrow{60℃,\,30\,min} \left[Ni(NO_3)_2 \cdot 4H_2O + Ni(NO_3)_2 \cdot 2H_2O + Ni_2(NO_3)_2(OH)_2 + Ni_3(NO_3)_2(OH)_4 + Ni(OH)_2\right] \xrightarrow{MEA,\,60℃,\,2h} 2\,NiO + 4NO_2 + O_2 + 12H_2O$$

2nd step: calcination reaxion.

$$Ni_3(NO_3)_2(OH)_4 \xrightarrow{400℃,\,2h} 2\,NiO + 4NO_2 + O_2 + 12H_2O$$

The original spin coating device developed in this study was provided by taking into account the speed ranges of the motors in conventional devices and other parameters of the coating processes. The experimental setup for the application of the custom-designed spin coating technique was prepared in detail and this mechanism is shown in Fig. 1. Firstly, a 12V powered micro DC motor that can operate at different speeds up to 6000 rpm was determined. The main carrier body where the mechanism will be placed was created. A special slot for the motor and channels for motor connections were created in the main body. The motor spindle shoe part was added to the motor. This part consists of two parts. The shoe that fits the motor perfectly and the rotation stand that this shoe will be placed into. A gap compatible with the shoe was left at the bottom of the rotation stand. On the upper part of the rotation stand, channels were created for substrate holder equipment where the substrate to be coated can be placed. Then the substrate holder part was added. The substrate holder consists of four adjustable holders (substrate clamping jaws) that will ensure the substrate is fixed in a balanced manner. The substrate clamping jaws are adjusted according to the size of the substrate by moving within the channels of the rotation stand. The jaws can be fixed and locked from above. Thus, the substrate is prevented from being thrown and displaced. The flexibility of the substrate holder mechanism allows different materials to be held by compression. Supporting part was placed on the main body and around the rotating stand in a way that would not prevent the stand from rotating. A protection cover was produced on this equipment to cover the entire system. A hole was left at the top center of the protection cover, which was large enough to drip the coating material. This cover allowed the coating material to drip onto the substrate surface and prevented the coating material from splashing out due to speed or excess. The motor was connected to an adjustable power supply via the connection channels on the main body. In this way, parameters such as the operating speed and operating time of the motor controlled and adjusted. Increasing the number of coated layers and changing the spin coating speed can affect not only the film thickness but also the morphological, crystallographic and surface properties of the film. In this study, the effects of different coating parameters on the crystallization, surface smoothness and nanoparticle distribution of NiO thin films were investigated. Thanks to the method we developed, which is an alternative to the spin coating techniques used in the thin film deposition process, we have introduced a new low-cost, vacuum-free spin coating technique to the literature.

Gas sensor tests were carried out in the gas chamber control system shown in Fig. 2. Here the gas inlet and outlet

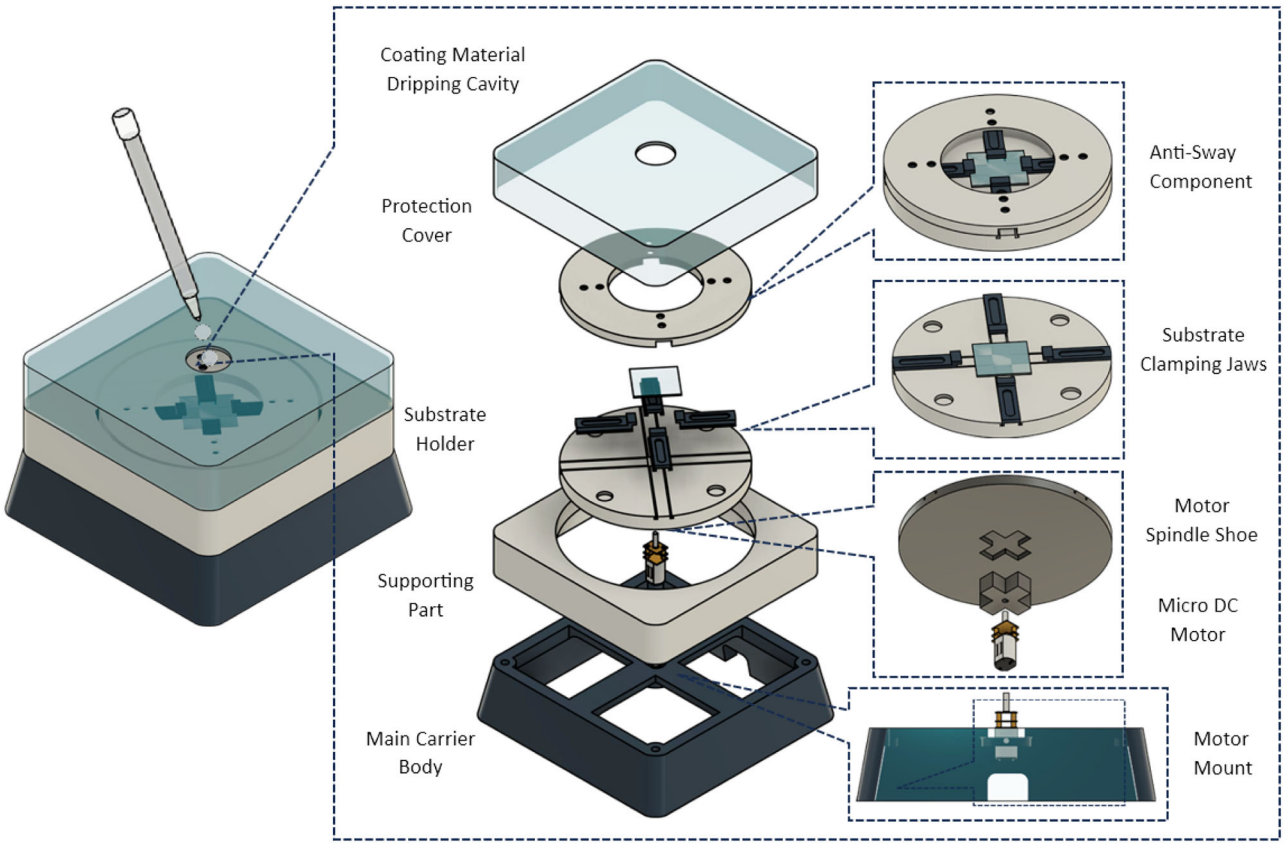

Fig. 1 Custom-designed spin coating mechanism for thin film deposition

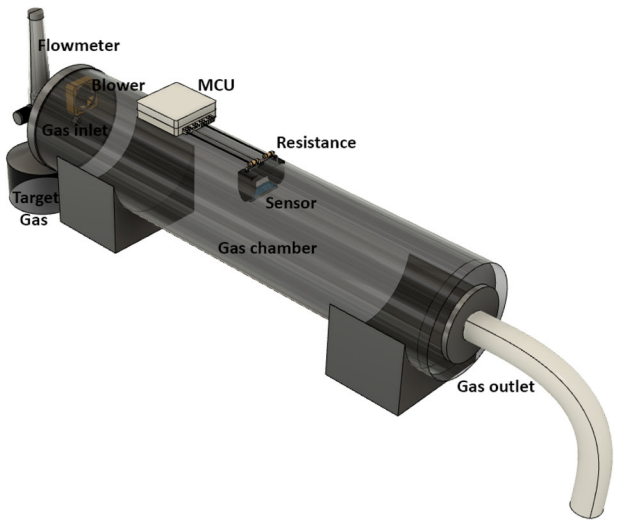

Fig. 2 Schematic representation of integrated gas chamber control system for gas sensor applications

lines are located on both sides of the chamber. The gas chamber is specially designed to ensure that the gas molecules interact with the sensor to give accurate and repeatable results. The volume of the designed gas chamber is 500 cm^3. With the gas inlet and outlet lines, the gas is evenly distributed in the chamber, reaches the sensor surface evenly and is discharged by the outlet valve after the tests. While the blower controls the gas flow, the flowmeter ensures precise measurement of the gas. When gas enters the chamber, the gas molecules moving towards the outlet side spread homogeneously in the chamber and then the outlet valve is opened and the gas is discharged. For the production of target gases, pure gases (ethanol, NO_2 and H_2) were obtained from commercially available cylindrical gas cylinders. Gas concentrations can be adjusted from 10 ppm to 500 ppm to monitor sensor reactions.

Figure 3 shows the electronic circuit diagram used for the gas sensor measurement performance evaluations. This circuit contains a microcontroller board (MCU) based measurement system and allows precise measurement of data from sensor samples in the gas chamber. The circuit is supplied with +5V and the measurement accuracy is provided by resistor elements (R1 and R2) that interact with the sensor. The voltage from the MCU first passes through the R1 resistor, then through the sensor sample and completes the circuit by following the path connected to the R2 and MCU board paths. Depending on the gas supplied to the chamber, the contact time, the resistances in the system and the sensors on the circuit, the variable data received analogue from the MCU are digitally transferred to the computer system. Here, sensor measurement result data are

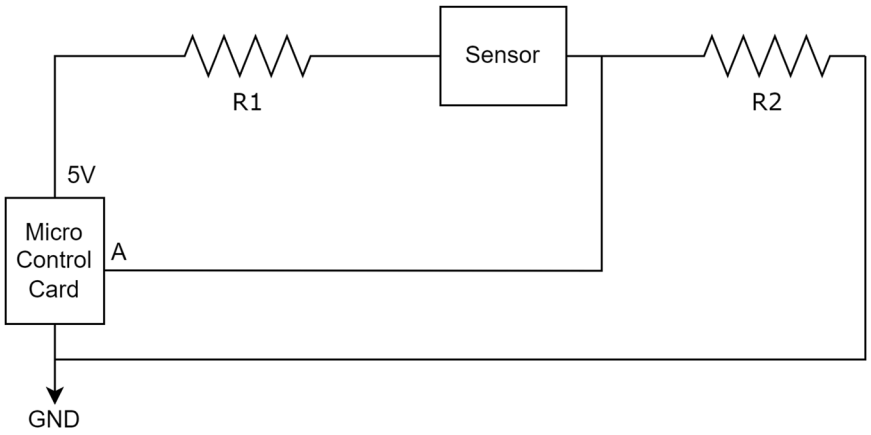

Fig. 3 Electronic circuit diagram for gas sensor response analysis

converted into graphs. The resistance and voltage values used in the circuit are designed to be adjustable depending on the needs or specified conditions. In this way, the system is made sensitive to small changes in the nanostructured NiO thin film sensor resistance in the presence of gas. In this study, the reaction changes of NiO coated glass samples against ethanol, NO_2 and H_2 gases were monitored by means of this system and the measurement performances of the gas sensor were evaluated.

3 Results and discussion

In order to determine the crystal structure of NiO thin films, X-Ray Diffractometer (XRD) measurements were carried out using Panalytical Empyrean device. Measurements were made with Cu-Kα (λ = 1.5406 Å) irradiation for high sensitivity in defining the crystal phases of thin films and evaluating the crystallization quality. The scans were performed in the range 20°≤2θ≤70°. and at a scanning speed of 2°/min. The XRD spectra of all series are given comparatively in Fig. 4. The spectra of the thin films were examined by comparison with the ICSD (Inorganic Crystal Structure Database) Number of: 98-009-2132 card of NiO in hexagonal structure. According to this examination, it is seen that all series are formed in polycrystalline structure, peaks belonging to hexagonal NiO are present in the spectrum and there is no other impurity peak different from the NiO structure in the spectrum. When the series are compared within themselves, it is understood that the crystallization in the series produced in 3 layers and 8 layers is lower than the series produced in 6 layers. In the 3-layer series, the (012) and (104) peaks are present in the series produced at 2000 rpm and 3000 rpm belonging to the hexagonal NiO structure, and only the (104) peak is present in the series produced at 4000 rpm. The intensities of these peaks are lower than in the series produced with 6 layers. The peak numbers and intensities in the 8 layer series are also lower than in the

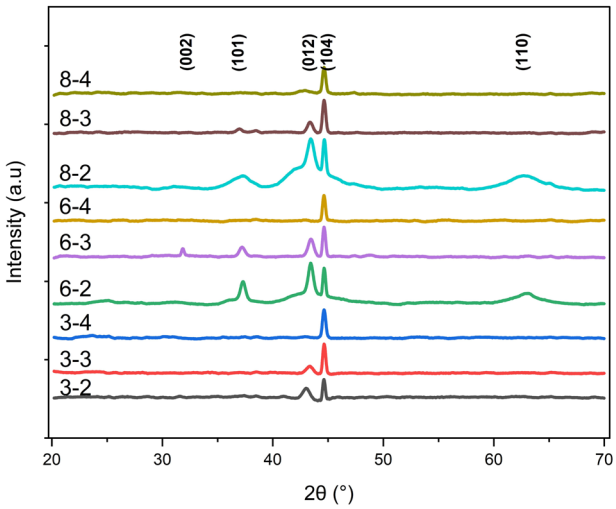

Fig. 4 XRD results of sensor samples

6 layer series. In addition, the full width half maximum (FWHM) values of the peaks in the 8 layer series are larger. These results also mean that crystallization is low. According to the same results, it was understood that 3 layers were not enough for good crystallization and 8 layers were too much. When the 6 layer series showing the best crystallization were evaluated among themselves, it was understood that the best crystallization was in the 6-3 series produced at 3000 rpm. This series contains the peaks (002), (101), (012) and (104) belonging to the hexagonal NiO structure, respectively. These comparisons confirm that the NiO films produced by the method used in the present study are consistent with the structural properties reported in the literature [60–65]. The only series in which these four peaks are present in the spectrum is the 6-3 series. The intensities of the peaks are higher and the FWHM values are lower than the other series.

The surface morphology and nanoparticle distribution of NiO thin films were examined with a Zeiss Supra 40 VP model Field Emission Scanning Electron Microscope

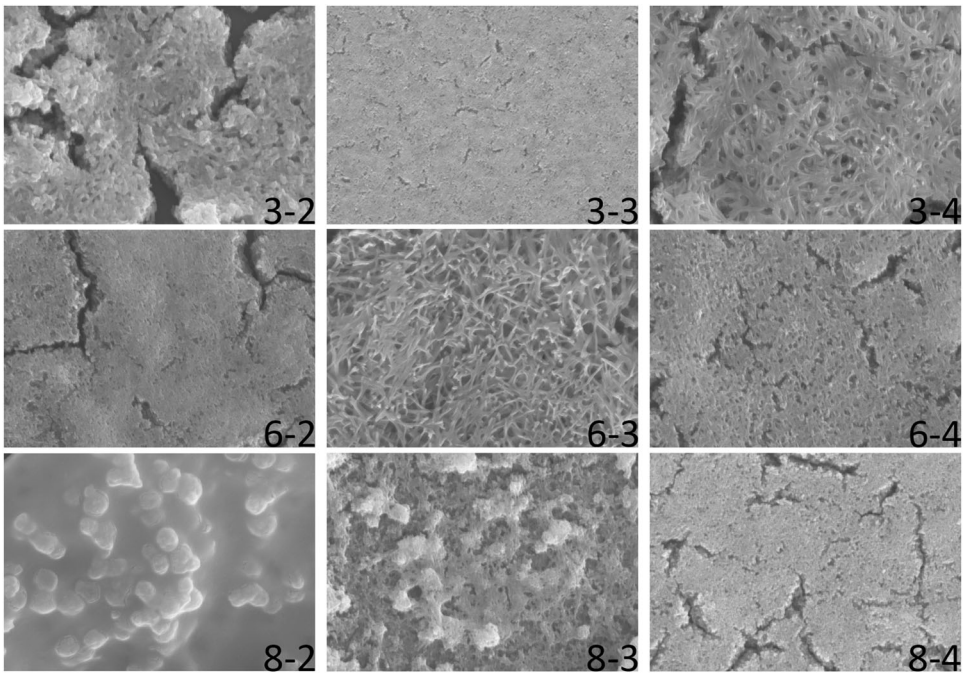

Fig. 5 SEM images of series

(FESEM). The instrument provides high resolution allowing the study of nanoscale features on the surface. During imaging, surface features such as surface homogeneity, particle distribution and agglomeration were evaluated.SEM images (30kx magnification) are shown in Fig. 5.

Images from the FESEM device were processed, colorized and 3D surface maps were created using Gwyddion software. with this software, surface roughness was detailed and topographic examinations were performed. These images are given in Fig. 6. In addition, average surface roughness values were calculated and their suitability for sensor applications was evaluated. When the images are examined, it is seen that the surfaces are not completely homogeneous in the 3 layer and 8 layer series, and that agglomerations occur in the formation of the 8 layer series. In the 6 layer series, it is seen that the thin film surface consists of nano particles, the particles are almost homogeneously distributed on the surface and there are no agglomerations. It is also noteworthy that the nano particles formed on the surface are formed in the needle-like structure of the NiO structure. The results obtained from these images support the conclusion that the best crystallization occurs in the 6 layer series, as determined in the XRD spectrum.

The average surface roughness values calculated for all series are shown in Table 2. The effects of the number of layers and rotational speed used during coating on the surface roughness were analysed. The average surface roughness was measured as 275.8 nm and 370.8 nm for samples 3-3 and 6-3, respectively. This indicates that a higher number of layers and an optimum rotational speed of 3000 rpm increase the roughness, providing a more suitable surface for sensor applications. Samples with 8 layers and 4000 rpm coating showed a decrease in roughness to 268.7 nm due to clustering or surface irregularities. These values are consistent with the roughness ranges reported in similar studies. [66–68] The average roughness value calculated as approximately 325 nm is a suitable value for sensor applications, which is another stage of our study.

When the +5V voltage given to the gas chamber control system passes through the semiconductor NiO sensors and reaches the MSU, the first voltage value on the system is read. Here, it is understood that the sensor is at a stable basic resistance level and there is no gas exposure. In all processes in gas sensor measurements, no gas is entered into the gas chamber for the first 180 s. Gas is supplied to the gas chamber for the next 180 s. In the next process, gas is discharged for 180 s and gas is entered again for the next 180 s. Gas entry and exit cycles were performed with 3 repetitions. In other words, the periods when gas is entered are the 180th second, 540th second and 900th second. As a result of gas sensor measurements, only stable and repeatable data was obtained in the 6-3 series. The poor performance of other series is due to factors such as surface agglomeration and poor crystallization. These factors negatively affected the interaction mechanism between the sensor surface and gas molecules. A reaction was obtained from this sample against 3 different gases [69–74]. Figure 7 shows the ethanol gas sensor measurement results for sample number 6-3. During the initial phase, up to 180 s, the sensor exhibited an average voltage of approximately 2.26 V and a resistance of $8.2 \times 10^3 \Omega$. When the first

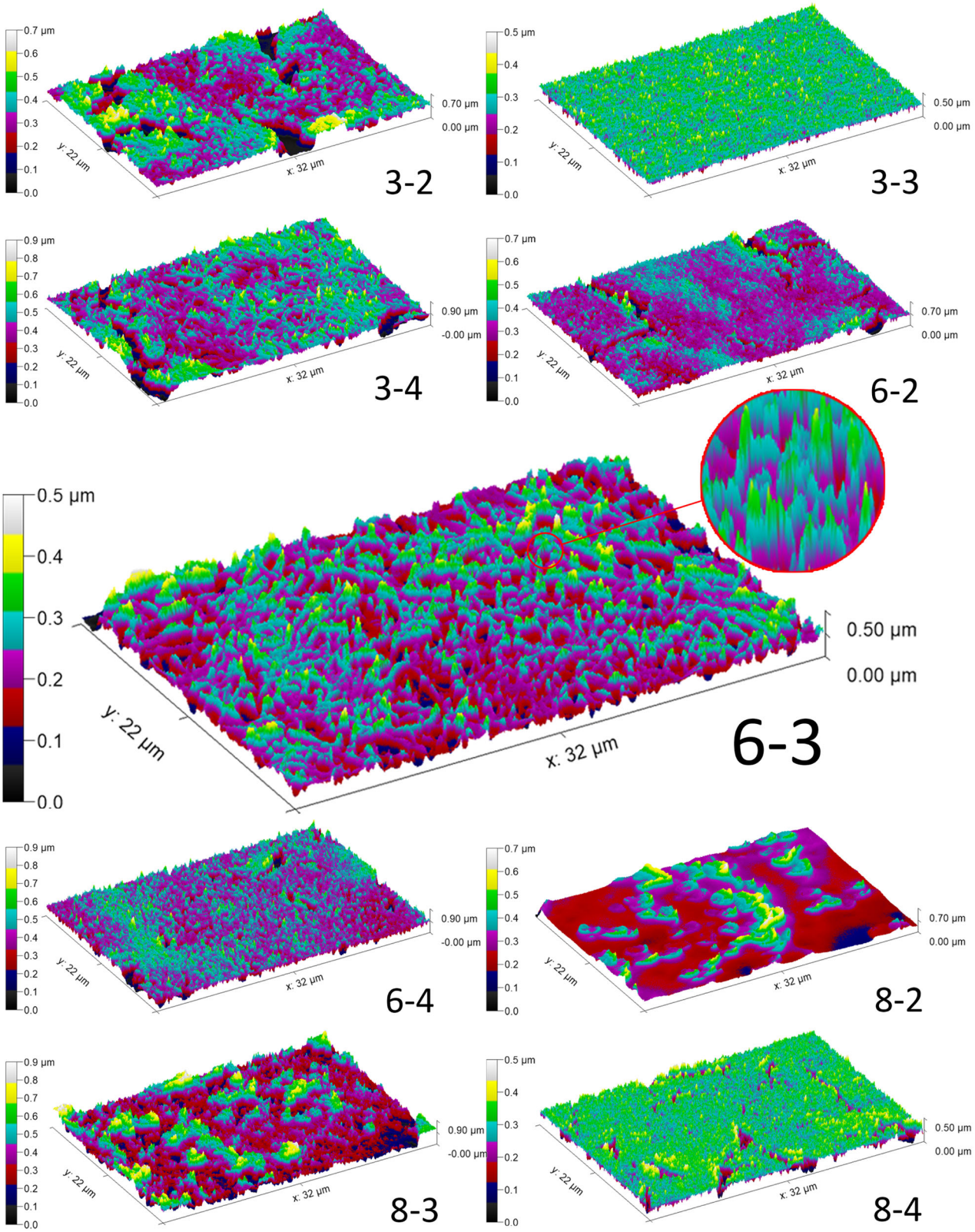

Fig. 6 AFM images of series

ethanol gas was introduced at 180 s, the voltage and resistance values rose rapidly. During the time the gas was in the chamber, the voltage approximately increased to 4.39 V and the resistance increased to $7.7 \times 10^5 \Omega$. This increase occurs because the NiO-based sensor is a *p*-type semiconductor. When ethanol gas interacts with NiO, it donates electrons and the hole concentration on the surface decreases, which causes the resistance to increase. [75–78] This process continues until the 360th second and a peak is seen in the graph at around 4.54 V. At the 360th second, ethanol gas is started to be discharged. In this case, the resistance of the sensor gradually decreases. During gas evacuation (360–540 s), the average resistance and voltage decreased to $9 \times 10^3 \Omega$ and 2.36 V, respectively, returning to their baseline levels. This decrease in resistance shows the process of the sensor surface returning to its original state as the gas is removed from the chamber. From the 370th second onwards, the value obtained from the port has approached the average voltage values before the gas was first introduced. However, these values are slightly higher than the initial level. This indicates that the sensor shows a slight increase before reaching full equilibrium. In the second (540–720 s) and third (900–1080 s) gas introduction-evacuation cycles, the sensor response became more stable compared to the first cycle. In these cycles, the voltage was consistently stable around 4.60 V during the gas presence and the resistance stabilized at about $12.3 \times 10^5 \Omega$. The initial cycle showed minor instability, but the subsequent cycles demonstrated a more homogeneous reaction, with the sensor providing a stable response. In each cycle, resistance increased during gas introduction and decreased during evacuation, indicating the sensor's reliable and repeatable performance.

Table 2 Average roughness measurements for different serial samples

Serial	Average Roughness (nm)
3-2	288.4
3-3	275.8
3-4	411.9
6-2	299.8
6-3	370.8
6-4	381.6
8-2	288.7
8-3	344.0
8-4	268.7

Figure 8 shows the changes in the voltage and resistance response of the NiO-based gas sensor with NO_2 gas over time. Initially, the output voltage on the resistor was observed to be approximately 2.33 V and the resistance was approximately 8.7 x $10^3 \Omega$, indicating the baseline conditions before NO_2 exposure. At 180 s, when NO_2 gas was introduced into the test chamber, a rapid decrease in the resistance and voltage values occurred. Adsorption of NO_2 onto the NiO surface interacts with the oxygen vacancies on the surface, increasing the hole density. This process leads to a decrease in the electrical resistance of the sensor, and thus the presence of NO_2 can be detected quickly and sensitively [79–83]. The sensor response reaches a negative peak but gradually stabilizes with time. This stabilization is probably due to the saturation of the active adsorption sites on the sensor surface, which slows down further reaction. The cyclic nature of the experiment, where NO_2 gas is

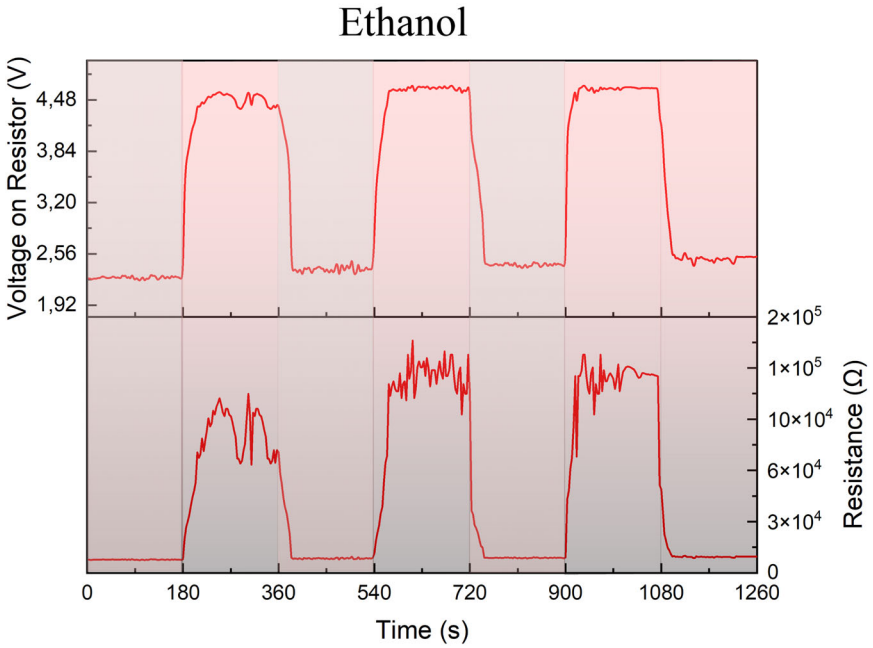

Fig. 7 Ethanol gas sensing response for sensor sample 6-3

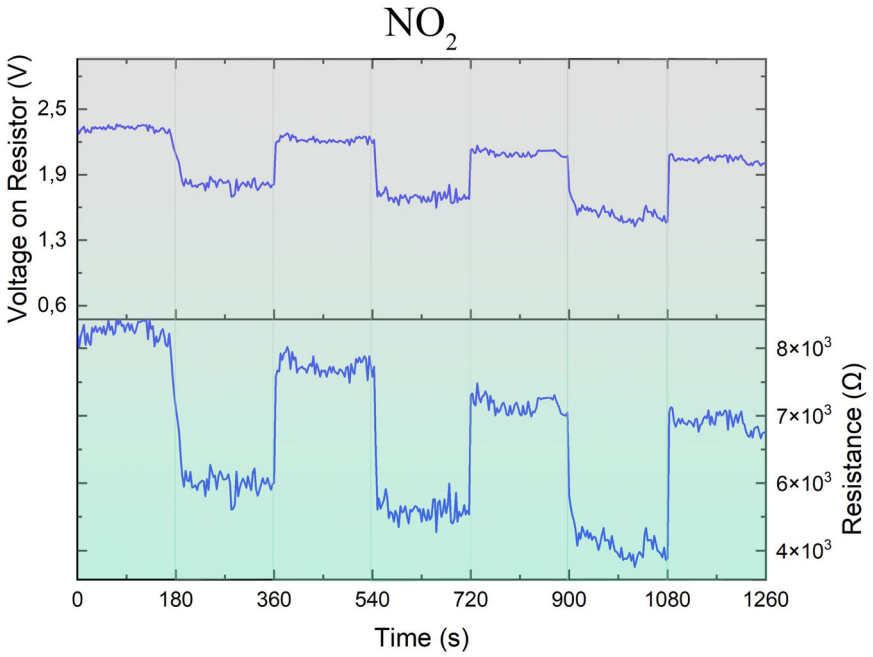

Fig. 8 NO_2 gas sensing response for sensor sample 6-3

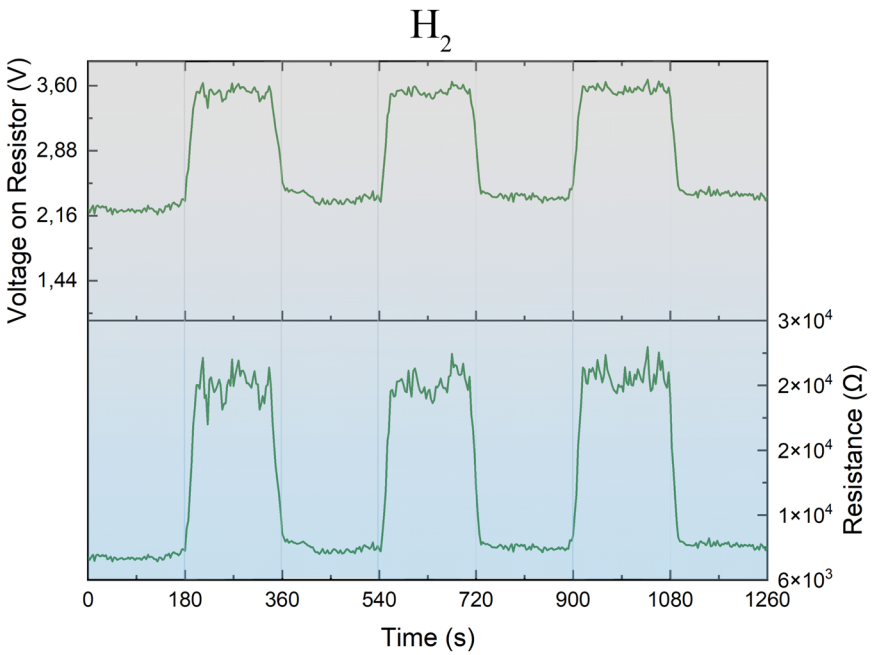

Fig. 9 H_2 gas sensing response for sensor sample 6-3

periodically removed and reintroduced (every 180 s), demonstrates the repeatable and reversible response of the sensor. Each NO_2 introduction results in a similar voltage and resistance decrease, highlighting the stability and repeatability of the sensor. Importantly, this cyclic pattern highlights the reliability of the sensor in detecting NO_2 gas, as the response remains consistent across multiple gas exposure cycles. The observed resistance values decrease from an average of 8 x $10^3\Omega$ to approximately 4-5 x $10^3\Omega$ during gas exposure, further confirming the sensitivity and response of the sensor.

Figure 9 shows the interaction of the NiO-based sensor with the introduction of H_2 gas into the gas chamber system. While a smooth voltage and resistance graph is observed for the first 180 s, these values increased from the moment H_2 gas was introduced to the gas chamber. Afterwards, until the 360th second, approximately 2.2 V voltage and 8 x $10^3\Omega$ resistance values were observed. This increase was again due to the reducing properties of H_2 gas, as in ethanol gas [84–87]. With the discharge of the gas from the medium, the sensor took values close to its initial values. These cycles were repeated in a similar way. While approximately

3.5 V voltage and 2.4 x $10^4\Omega$ resistance values were observed in the total periods when there was gas inlet, the voltage took an average value of 2.3 V and the resistance took an average value of 8.6 x $10^3\Omega$ during the periods when there was no gas in the gas chamber.

Structural and morphological properties of the material are decisive on sensor performance. From XRD analyses, it was observed that NiO films in the 6-3 series crystallize optimally on the surface. This allowed gas molecules to interact more effectively with the surface. AFM and SEM results confirm that this sample has homogeneous surface structure and suitable roughness value. The sensor results show that as a result of these structural and surface properties, stable measurability and reproducibility of gas sensing in the 6-3 series were detected. This correlation explains that the gas sensing mechanism is directly linked to the material properties. In the study conducted on the gas sensing performance of NiO thin film sensors, it was determined that the resistance and voltage change trends of the sensors against gases with reducing properties (ethanol and H_2) followed a similar course over time, but their reaction intensities differed. In particular, it was observed that the sensors exhibited the highest change in terms of reaction percentage when exposed to ethanol gas. Ethanol was followed by H_2 and NO_2 gases, respectively. In this context, the response of 6-3 series NiO thin film sensors can clearly distinguish between the presence and absence of gas against three types of gas. This behavior indicates that the gas detection performance of the sensor is reliable and remains stable over repeated cycles. In addition, the fast detection and recovery times of the 6-3 series increase the potential of the sensor to be used both in dynamic gas sensing conditions and in long-term applications. In conclusion, this study highlights the sensitivity of NiO thin films to gases such as ethanol, H_2 and NO_2 in terms of gas sensing performance and especially the positive effect of optimized structural features of 6-3 series on sensor stability. These findings indicate that NiO-based gas sensors may have a wide range of potential applications.

4 Conclusion

In this study, NiO thin films were successfully deposited on glass substrates using a novel spin coating technique, which was developed as a cost-effective and vacuum-free alternative to traditional methods. The structural and morphological analysis of the films, as assessed by XRD and FESEM, revealed that the optimal crystallization and surface homogeneity were achieved with the 6-layer sample coated at 3000 rpm. This sample demonstrated good crystallization with distinct NiO peaks and well-distributed nanostructures, confirming the effectiveness of the new spin coating method. The gas sensor tests performed on the 6-3 sample showcased its sensitivity and repeatability in detecting ethanol, NO_2, and H_2 gases. The sensor exhibited a stable response across multiple gas exposure cycles, highlighting its potential for reliable gas detection applications. The NiO sensor's ability to distinguish between different gases and return to baseline resistance after gas removal indicates its practicality for use in environmental monitoring and other industrial applications. Overall, the results suggest that the newly developed spin coating device is a viable alternative to conventional spin coating techniques, offering comparable performance with added benefits of lower cost and operational simplicity. This advancement opens up possibilities for broader applications in thin film deposition and gas sensor technology, contributing valuable methodologies to the existing literature.

Data availability

No datasets were generated or analysed during the current study.

Supplementary information The online version contains supplementary material available at https://doi.org/10.1007/s10971-025-06678-9.

Author contributions EN undertook the roles of conceptualization, investigation, material synthesis, methodology, experimentation, visualization, writing-review and editing. MFG focused on methodology, validation, visualization, framing, experimentation, and writing-review. BA contributed to device modeling, visualization, experimentation. ST contributed to methodology, validation, formal analysis, writing-review, experimentation, material characterization and validation. FOG handled validation, formal analysis along with writing-review and editing duties.

Funding This research was conducted without any funding. Open access funding provided by the Scientific and Technological Research Council of Türkiye (TÜBİTAK).

Compliance with ethical standards

Conflict of interest The authors declare no competing interests.

Ethical approval This review does not involve any procedures that raise ethical issues or require institutional approval.

References

1. Feng T, Sun Y, Shi Y, Ma J, Feng C, Chen Z (2024) Air pollution control policies and impacts: A review. Renew Sustain Energy Rev 191:114071
2. Sharma S, Barman T, Mishra G, Kumar A (2024) Micro and nanoplastics pollution: A review on global concern and its impacts on ecosystems. Land Degrad Dev 35(9):2963–2981
3. Wang L, Chen L (2024) Resource dependence and air pollution in China: Do the digital economy, income inequality, and industrial upgrading matter? Environ Dev Sustain 26(1):2069–2109
4. Filonchyk M, Peterson MP (2024) Analysis of air pollution from vehicle emissions for the contiguous United States. J Geovisualization Spat Anal 8(1):16
5. Kanth S, Choudhury S, Kumar S, Rao R, Debnath A, Betty C (2024) Reliable NO_2 sensing and alert system based on pd-pdo thin film with sub ppm level detection at room temperature. Sens Actuators B Chem 403:135145
6. Su H, Yang H, Ma C, Tang J, Zhu C, Wang X, Zeng D (2024) High response and selectivity of the sno2 nanobox gas sensor for ethyl methyl carbonate leakage detection in a lithium-ion battery. ACS Sens 9(1):444–454
7. Perillo P, Rodriguez D (2024) Cds thin film sensor for NO_2 and H_2S detection at room temperature. Appl Phys A 130(6):372
8. Babbar D, Garg N, Kabra S (2024) Comparative simulation study of ingan and silicon channel stack oxide twin gate field effect transistor based ammonia gas sensor. Sens Imaging 25(1):20
9. Nithya S, Devi YR, Dutta A (2024) Synthesis and characterization of α-Fe_2O_3 nanoparticles for high-performance co gas sensor. Emergent Mater 7:1793–1804
10. Zhang M, Lv X, Wang T, Pei W, Yang Y, Li F, Yin D, Yu H, Dong X (2024) Cuo-based gas sensor decorated by polyoxometalates electron acceptors: From constructing heterostructure to improved sensitivity and fast response for ethanol detection. Sens Actuators B Chem 415:136016
11. Pan Z, Wang D, Zhang D, Yang Y, Yu H, Wang T, Dong X (2024) RGO doped MOFs derived α-Fe_2O_3 nanomaterials for self-supporting ppb-level NO_2 gas sensor. Sens Actuators B Chem 405:135378
12. Xu S, Hu J, Zhu D, Cheng M, Wei T, Liu Q, Wang R, Li W, Ling Y, Liu B (2024) Design of Ag modified Cu@ Cu_2O/CuO hierarchical heterostructure hybrid for high-performance room temperature NO_2 sensing. J Mater Sci Mater Electron 35(9):647
13. Merah SM, Bakha Y, Djelloul A (2024) N-type and p-type SNOX thin films based mox gas sensor testing. J Mater Sci Mater Electron 35(3):250
14. Gozukizil MF, Nayman E, Temel S, Gokmen FO (2024) Comparison of gas sensing performances in various yarn types coated with polyaniline. J Mater Sci Mater Electron 35(7):529
15. Kumar M, Saravanan A, Joshi SA, Chen S-C, Huang B-R, Sun H (2024) High-performance self-powered uv photodetectors using sno2 thin film by reactive magnetron sputtering. Sens Actuators A Phys 373:115441
16. Jácome-Martínez C, Márquez-Marín J, Olvera-Amador MDLL, Castanedo-Pérez R, Torres-Delgado G (2024) Cuo thin films deposited by the dip-coating method as acetone vapor sensors: Effect of their thickness and precursor solution molarity. Micro Nanostruct 187:207753
17. Alaghmandfard A, Fardindoost S, Frencken AL, Hoorfar M (2024) The next generation of hydrogen gas sensors based on transition metal dichalcogenide-metal oxide semiconductor hybrid structures. Ceram Int 50(17):29026–29043
18. Temel S, Gokmen FO, Yaman E (2020) Antibacterial activity of ZnO nanoflowers deposited on biodegradable acrylic acid hydrogel by chemical bath deposition. Bull Mater Sci 43:1–6
19. Gozukizil M, Nayman E (2024) Deposition of cdo thin films by dip coating technique and the effect of concentration on gas sensor applications. Latin Am Appl Res 54(1):119–125
20. Rojano Chávez SM, Ayala LM, Karthik TVK, Maldonado A, Gómez-Pozos H (2024) Zinc oxide thin films deposited by sol–gel spin-coating technique for propane and carbon monoxide sensing applications. J Mater Sci Mater Electron 35(11):797
21. Nayman E, Gözükızıl MF, Usta İ (2023) Deposition of cdo semiconductors on yarns by dip coating method and gas sensor applications. Text Appar 34(2):117–126
22. Hammad ABA, Nahrawy AME, Mansour A (2024) Structural and optical properties of sol–gel-spin coating nanostructured cadmium zinc nickel phosphate (CZNp) film and the current transport properties of CZNp/p-si-based diode. Silicon 16(5):2049–2063
23. Temel S, Nebi M, Peker D (2018) Optical band gap engineering of (MgO) x (ZnO) 1-x films deposited by sol-gel spin coating. Optoelectron Adv Mater Rapid Commun 12(1-2):76–79
24. Nebi M, Peker D, Temel S (2018). Deposition of Co doped TiO_2 films using sol gel spin coating technique and investigation of band gap. In *AIP Conference Proceedings*, volume 1935. AIP Publishing.
25. Temel S, Gozukizil F, Gokmen FO, Yaman E (2023) Comparison of gas sensor properties by producing ZnO thin films with different techniques. J Optoelectron Adv Mater 25:282–288
26. Chandak V, Kumbhar M, Talekar S, Gunjakar J, Kulal P (2024) Ultrasensitive and selective cr-doped ZnO thin films synthesized via spray pyrolysis technique for detection of ammonia gas. Appl Phys A 130(5):285
27. Temel S, Gokmen F, Yaman E (2017) Effects of deposition time on structural and morphological properties of synthesized ZnO nanoflowers without using complexing agent. Eur Sci J 9:13–27
28. Temel S, Gökmen FÖ, Yaman E (2019) An energy efficient way to produce zinc-based semiconductor thin films via chemical bath deposition technique. J Sustain Dev Energy Water Environ Syst 7(2):253–260
29. Tohidi T, Novini NY, Jamshidi-Galeh K (2024) Effect of gamma irradiation on optical characteristics of fe-doped CDs thin films prepared using chemical bath deposition. Opt Mater 151:115394
30. Crivello C, Sevim S, Graniel O, Franco C, Pané S, Puigmartí-Luis J, Muñoz-Rojas D (2021) Advanced technologies for the fabrication of MOF thin films. Mater Horiz 8(1):168–178
31. Natashah FA, Hisamuddin SN, Coffey AH, Zhu C, Bawazeer TM, Alsoufi MS, Roslan NA, Supangat A (2024) Edge-on orientation of thermally evaporated metal phthalocyanines thin films for humidity sensing application. J Mater Sci Mater Electron 35(7):512
32. Ziaei S, Es'haghi Z (2024) Combination of chemical vapor deposition and thermal growth methods for facile synthesis of tin oxide-doped multiwalled carbon nanotubes. J Iran Chem Soc 21(5):1403–1411
33. Horoz B, Tuna Yıldırım S, Soltabayev B, Ateş A, Acar S, Yıldırım MA (2024) Effect of silar cycle on gas sensing properties of In_2O_3 thin films for co gas sensor. J Mater Sci Mater Electron 35(2):163
34. Taha T, Saad R, Zayed M, Shaban M, Ahmed AM (2023) Tuning the surface morphologies of ZnO nanofilms for enhanced sensitivity and selectivity of co2 gas sensor. Appl Phys A 129(2):115
35. Nouasria FZ, Selloum D, Mokrani OBE, Fenniche F, Tingry S, Khane Y, Henni A, Belkhalfa H, Dizge N, Albukhaty S et al. (2024). In-depth study of chemically electrodeposited cuprous oxide (Cu_2O) thin films on ITO glass. Plasmonics, 1–11.
36. Aydas B, Atılgan A, Ajjaq A, Acar S, Öktem MF, Yildiz A (2024) Flexible NH3 gas sensors based on ZnO nanostructures deposited on kevlar substrates via hydrothermal method. Ceram Int. 50(18):32477–32489

37. Mala S, Latha H, Udayakumar A (2024) Design and fabrication of indium tin oxide based thin film piezoresistive pressure sensor. Exp Tech 48:761–773
38. Karimi Z, Sadeghi A, Ghaffarinejad A (2023) The comparison of different deposition methods to prepare thin film of silicon-based anodes and their performances in li-ion batteries. J Energy Storage 72:108282
39. Ilickas M, Marčinskas M, Peckus D, Mardosaitė R, Abakevičienė B, Tamulevičius T, Račkauskas S (2023) ZnO UV sensor photoresponse enhancement by coating method optimization. J Photochem Photobiol 14:100171
40. Zhao Z, Ma S, Rahmatullah ABM, Chen Z, Pan Y, Wu L, Huang B (2024) Flexible gas-strain dual sensor based on pu-supported ti3c2tx/ceo2/tio2 yarns. Mater Sci Semicond Process 181:108607
41. Kumar V, Adalati R, Gautam YK, Gautam D (2024) An investigation of glass, ito, and quartz transparent substrates on Pd/SnO_2 hydrogen sensor structure and sensitivity. Mater Today Commun 40:109280
42. Li Y, Zhang B, Li J, Duan Z, Yang Y, Yuan Z, Jiang Y, Tai H (2024) Pd-decorated ZnO hexagonal microdiscs for NH3 sensor. Chemosensors 12(3):43
43. Chakraborty B, Litra D, Mishra AK, Lupan C, Nagpal R, Mishra S, Qiu H, Railean S, Lupan O, De Leeuw NH (2024) Ultra-selective hydrogen sensors based on CuO-ZnO hetero-structures grown by surface conversion. J Alloy Compd 1002:175385
44. Şakar BC, Kundakçı M (2024) Structural, optical, electrical and gas sensor properties of fe-doped cdo thin films synthesized by spray pyrolsis. Ceram Int 50(3):4589–4599
45. Zhang Z, Zheng Z, He X, Liu K, Debliquy M, Zhou Y, Zhang C (2024) Electronic nose based on metal oxide semiconductor sensors for medical diagnosis. Prog Nat Sci Mater Int 34(1):74–88
46. Goel R, Jha R, Ravikant C (2023) Nickel oxide (NiO) nanotriangles with enhanced electrochromic and photovoltaics properties. Chem Pap 77(5):2885–2903
47. Bogachuk D, Baretzky C, Eckert J, Yang B, Suo J, Dangudubiyyam UK, Loukeris G, Mohammadzadeh H, Kluska S, Kohlstädt M (2024) Rethinking electrochemical deposition of nickel oxide for photovoltaic applications. Sol RRL 8(2):2300750
48. Arjun V, Muthukumaran K, Nithya A, Yoshimura M, Karuppuchamy S (2024) Nickel oxide incorporated $CH_3NH_3PbI_3$ for stable and efficient planar perovskite solar cells. Sol Energy Mater Sol Cells 271:112857
49. Ahmad R, Shah M (2023) Nickel oxide (NiO) nanoflakes prepared through hydrothermal method and integration into acetone gas sensing application. Chem Pap 77(1):413–421
50. Wang M, Liu H, Sun C, Pan G, Yang X, Shao J, Dong J, Qi Y (2024) High efficiency toluene sensor based on iron-doped nickel oxide triple-shell microspheres with high moisture resistance. Mater Sci Eng B 299:117001
51. Mohammad MJ, Sudha A, Adavalli MH, Swaminathan P (2023) Room temperature chemiresistive sensing of carbon dioxide using a composite of zinc oxide and nickel oxide. Surf Interfaces 41:103155
52. Pehlivanoglu SA (2021) Fabrication of p-si/n-nio: Zn photodiodes and current/capacitance-voltage characterizations. Phys B Condens Matter 603:412482
53. Arif B, El-Nasser H, Dere A, Al-Ghamdi AA, Bin-Omran S, El-Tantawy F, Yakuphanoglu F (2015) Optical properties of zn 1- x al x o: Nio transparent metal oxide composite thin films prepared by sol–gel method. J Sol-Gel Sci Technol 76:378–385
54. Souissi M, Schmerber G, Colis S, Alruwaili M (2023) Study of Zn1- 2xnixfexo thin films coated on glass by sol–gel spin-coating method for DMS materials. Eur Phys J 138(8):716
55. Nayman E, Gözükızıl MF, Usta İ (2024) Deposition of cdo semiconductors on yarns by dip coating method and gas sensor applications. Text Appar 34(2):117–126
56. Gözükızıl MF, Nayman E (2023) Co_2 gaz sensörü uygulamaları için cuo i˙nce film üretimi ve karakterizasyonu. Düzce Üniversitesi Bilim ve Teknol Derg 11(4):2246–2254
57. Gözükızıl MF, Temel S, Özbay N (2020) Production and characterization of al-doped ZnO thin films with sol-gel magnetic spin coating technique. Sakarya Univ J Sci 24(1):172–177
58. Estellé J, Salagre P, Cesteros Y, Serra M, Medina F, Sueiras J (2003) Comparative study of the morphology and surface properties of nickel oxide prepared from different precursors. Solid State Ion 156(1-2):233–243
59. Yang Q, Sha J, Ma X, Yang D (2005) Synthesis of NiO nanowires by a sol-gel process. Mater Lett 59(14-15):1967–1970
60. Dhas SD, Maldar PS, Patil MD, Nagare AB, Waikar MR, Sonkawade RG, Moholkar AV (2020) Synthesis of nio nanoparticles for supercapacitor application as an efficient electrode material. Vacuum 181:109646
61. Narang AD, Gupta SP, Sanap PP, Kahandal SS, Tupke RS, Kim H, Wang Q, Vedpathak AS, Sartale SD, Gade VK (2024) Development of nickel oxide thin film by chemical route for supercapacitor application. J Mater Sci Mater Electron 35(19):1335
62. Olajire A, Mohammed A (2020) Green synthesis of nickel oxide nanoparticles and studies of their photocatalytic activity in degradation of polyethylene films. Adv Powder Technol 31(1):211–218
63. Ezhilarasi AA, Vijaya JJ, Kaviyarasu K, Zhang X, Kennedy LJ (2020) Green synthesis of nickel oxide nanoparticles using solanum trilobatum extract for cytotoxicity, antibacterial and photocatalytic studies. Surf Interfaces 20:100553
64. Hammad AH, Abdel-Wahab MS, Vattamkandathil S, Ansari AR (2019) Growth and correlation of the physical and structural properties of hexagonal nanocrystalline nickel oxide thin films with film thickness. Coatings 9(10):615
65. Akshhayya C, Okla MK, Al-ghamdi AA, Al-amri SA, Alatar AA, Abdel-Maksoud MA, Aufy M, Khan SS (2023) Nano-architecture of intimate n-cufe2o4 coupled p-nio for enhanced white light photocatalysis: kinetics and intrinsic mechanism. J Clust Sci 34(5):2459–2469
66. Srinivasa N, Haunsbhavi K, Srinatha N, Mahesh H, Valanarasu S, Angadi B (2024) Investigation of sensing properties of sn-doped nio thin films for the detection of ammonia gas. Mater Sci Eng B 301:117178
67. Aftab M, Butt MZ, Ali D, Tanveer MU, Hussnain A (2020) Effect of molarity on the structure, optical properties, and surface morphology of (002)-oriented ni2o3 thin films deposited via spray pyrolysis: Effect of molarity on the properties of Ni_2O_3 thin films. Proc Pak Acad Sci A Phys Comput Sci 57(2):51–74
68. Gomaa M, Sayed M, Patil V, Boshta M, Patil P (2021) Gas sensing performance of sprayed nio thin films toward NO_2 gas. J Alloy Compd 885:160908
69. GangaReddy K, Nagaraju P, Reddy G, Ghosal P, Reddy MR (2022) Growth and characterization of electron beam evaporated nio thin films for room temperature formaldehyde sensing. Sens Actuators A Phys 346:113876
70. Benedict S, Singh M, Naik TR, Shivashankar S, Bhat N (2018) Microwave-synthesized nio as a highly sensitive and selective room-temperature NO_2 sensor. ECS J Solid State Sci Technol 7(7):Q3143
71. Zhang J, Wu C, Li T, Xie C, Zeng D (2020) Highly sensitive and ultralow detection limit of room-temperature no2 sensors using in-situ growth of PPY on mesoporous NiO nanosheets. Org Electron 77:105504
72. Kim H-J, Lee J-H (2014) Highly sensitive and selective gas sensors using p-type oxide semiconductors: overview. Sens Actuators B Chem 192:607–627
73. Yang B, Myung NV, Tran T-T (2021) 1d metal oxide semiconductor materials for chemiresistive gas sensors: a review. Adv Electron Mater 7(9):2100271

74. Kaur N, Zappa D, Comini E (2019) Shelf life study of nio nanowire sensors for No2 detection. Electron Mater Lett 15:743–749
75. Shailja, Singh K, Singh RC (2021) Highly sensitive and selective ethanol gas sensor based on ga-doped nio nanoparticles. J Mater Sci Mater Electron 32(8):11274–11290
76. Feng C, Kou X, Chen B, Qian G, Sun Y, Lu G (2017) One-pot synthesis of in doped nio nanofibers and their gas sensing properties. Sens Actuators B Chem 253:584–591
77. Taeño M, Maestre D, and Cremades A (2020) Fabrication and study of self-assembled nio surface networks assisted by sn doping. J Alloy Compd 827:154172
78. Li Q, Zeng W, Li Y (2022) Nio-based gas sensors for ethanol detection: Recent progress. J Sens 2022(1):1855493
79. Ambi R, Mane A, Tasgaonkar R, Mane R (2024) Highly porous nio microstructure for NO_2 detection. Phys B Condens Matter 674:415567
80. Li Z, Li H, Wu Z, Wang M, Luo J, Torun H, Hu P, Yang C, Grundmann M, Liu X (2019) Advances in designs and mechanisms of semiconducting metal oxide nanostructures for high-precision gas sensors operated at room temperature. Mater Horiz 6(3):470–506
81. Berwal P, Rani S, Sihag S, Singh P, Bulla M, Jatrana A, Kumar A, Kumar A, Kumar V (2024) Fabrication of NiO based thin film for high-performance NO_2 gas sensors at low concentrations. Phys B Condens Matter 685:416023
82. Ambi R, Mane A, Patil V, Mane R (2024) Highly porous hierarchical nio coated ZnO PN heterostructure for NO_2 detection. Mater Sci Eng B 300:117066
83. Luan VH, Tien HN, Hur SH, Han JH, Lee W (2017) Three-dimensional porous nitrogen-doped nio nanostructures as highly sensitive NO_2 sensors. Nanomaterials 7(10):313
84. Sakar Ceviz B (2024) H2 gas response of nio thin film at different gas concentrations. Turk J Nature Sci 10(1):77–81
85. M'hammedi K, Talbi L, Berouaken M, Manseri A, Gabouze N (2024) Hydrogen gas sensor based on nio decorated macroporous silicon heterojunction. Bull Mater Sci 47(3):210
86. Pai SHS, Mondal A, Ajitha B, Reddy YAK (2024) Effect of calcination temperature on NiO for hydrogen gas sensor performance. Int J Hydrog Energy 50:928–941
87. Nakate UT, Ahmad R, Patil P, Yu Y, Hahn Y-B (2020) Ultra thin NiO nanosheets for high performance hydrogen gas sensor device. Appl Surf Sci 506:144971